Network properties of the mammalian circadian clock

Rohling, J.H.T.

Chapter 4

Phase resetting caused by rapid shifts of small population of ventral SCN neurons

4.1 Introduction

Jet lag is often experienced as a disruption of day to day rhythms. The symptoms associated with jet lag are fatigue, reduced alertness and concentration, fragmented sleep, premature awakening, excessive sleepiness, and a decrement in performance (Waterhouse et al., 2007;Sharma, 2007). The symptoms can be caused by shift work, sleep disturbance or by acute time zone transitions caused by transatlantic flight (Reddy et al., 2002). Jet lag is attributed to slow adaptation of the circadian pacemaker, as well as to an unequal speed in the resetting of bodily functions (Takahashi et al., 2002).

In mammals, the suprachiasmatic nuclei (SCN) of the anterior hypothalamus drive daily rhythms. By means of a transcriptional and translational negative feedback loop, individual neurons of the SCN have endogenous circadian rhythms (Reppert and Weaver, 2001;Welsh et al., 1995). The individual neurons of the SCN synchronize in certain, not fully identified ways to produce a precise circadian rhythm at the tissue level (Enright, 1980a;Aton and Herzog, 2005;Colwell, 2005). The SCN receive information from the environmental light-dark cycle via specialized photoreceptors and pathways (Moore and Lenn, 1972;Morin and Allen,

2006). Under influence of light, the SCN synchronizes to the 24 hour environmental cycle (Quintero et al., 2003;Yamaguchi et al., 2003;Schaap et al., 2003;Brown et al., 2005a;Rohling et al., 2006b;VanderLeest et al., 2007).

Following a shift of the light-dark cycle, the circadian system requires several days to readjust to the new cycle. It is well known that adjustment of the circadian clock takes longer for eastbound flights, causing advances of the light-dark cycle, than for westbound flights, which cause delays.

Previous real-time electrical-activity measurements in SCN slices following a 6 hour delay of the light-dark cycle revealed bimodal patterns, with one shifted and one unshifted component (Albus et al., 2005). It appeared that the ventral part of the SCN corresponded with the rapidly shifting component while the dorsal region corresponded with the unshifted component (Albus et al., 2005). The aim of the present study is to provide a quantitative analysis of the observed bimodal electrical activity pattern.

We performed electrical activity recordings in SCN slices following a shift of the light-dark cycle and confirmed the presence of bimodal electrical activity patterns. Analysis of the bimodal activity records shows that the unshifted component is relatively broad and the shifted component narrower. Computer studies, including curve fitting analysis, show that the number of action potentials that contribute to the shifted component is a small fraction of those that contribute to the unshifted component. Subpopulation analysis confirms these findings, and shows strong synchronization in peak phase in the shifted component but not in the unshifted component. We propose that phase shifts are brought about by an initial rapid shift of a relatively small subpopulation of neurons within the SCN.

4.2 Methods

4.2.1 In vitro electrophysiology

All experiments were performed under the approval of the Animal Experiments Ethical Committee of the Leiden University Medical Center. Male wildtype Wistar rats (Harlan, Horst, The Netherlands) were individually housed in cages that were equipped with a running wheel and

entrained to a 12:12 light-dark cycle. Food and water were available ad libitum. When the animals were properly entrained, the light-dark schedule was delayed by 6 hours by delaying the time of lights-off (Albus et al., 2005). After subsequent exposure to one complete shifted light-dark cycle, the animals were killed by decapitation at the time of lights off. Brains were rapidly dissected from the skull and coronal hypothalamic slices (~400 µm thickness) containing the SCN were prepared and transferred to a laminar flow chamber within 6 min after decapitation. Slices were perfused with oxygenated artificial cerebrospinal fluid (ACSF) and kept at a temperature of 35°C. The slice was kept submerged and was stabilized with an insulated tungsten fork. We used one slice per animal.

The slices settled in the recording chamber for ~ 1 h before electrode placement. Recording electrodes were placed in the ventral and dorsal SCN in order to obtain multiunit discharge activity patterns from both SCN regions simultaneously. Action potentials were recorded with 90% platinum 10% iridium 75 µm electrodes, amplified 10k times and bandpass filtered (300 Hz low, 3 kHz high). The action potentials crossing a preset threshold well above noise (~5 µV) were counted electronically in 10s bins by a computer running custom made software. Time of occurrence and amplitudes of action potentials were digitized and recorded by a data acquisition system (Power1401, Spike2 software, CED, Cambridge, UK) and stored for offline analysis.

4.2.2 Analysis of in vitro electrophysiology

Multiunit activity data that showed two peaks on day 1 after the delay were used for analysis. The recordings were smoothed using a penalized least squares algorithm (Eilers, 2003). The data from dorsal and ventral SCN were pooled. The widths for both peaks of the bimodal pattern were determined at the height of the trough between both peaks. A straight line was drawn from the trough between the two peaks to the opposing slope of the peak to determine the width of the peak. To allow for comparison between different experiments, we also calculated the relative peak width. The difference in absolute and relative peak widths was tested for statistical significance with independent t tests ($p < 0.001$).

4.2.3 Subpopulation studies

Activity of neuronal subpopulations in the SCN was analyzed using MATLAB (Matlab, 2007). Subpopulations in the multiunit recordings were constructed on the basis of spike amplitude, and correlated with distance to electrode tip. The amplitude data were divided into 50 equally sized bins reaching from a low spike threshold level, representing a large number of neurons, to the highest threshold including only a few units (Schaap et al., 2003). Population and subpopulation activity were smoothed and the peak times of the different subpopulations were determined relative to the time of the trough between the shifted and the unshifted component in the multiunit activity recording. All experiments were aligned to the time of the troughs.

4.2.4 Peak fitting

To determine the relative contribution in electrical activity for each component, the area under the curve was determined for each component using manual curve fitting and automatic curve fitting procedures (Igor: http://www.wavemetrics.com and Origin: http://www.originlab.com). We fitted one peak for each component in the electrical activity multiunit pattern. In the manual curve fitting method we manually determined the peak for each component in the multiunit activity pattern. We defined a start time and an end time of the peak. Then we counted the number of action potentials in the region from the start time until the end time of the peak. The number of action potentials found for each peak represents the area for each component (see also figure 4.3). For each component the component peak area was taken as a relative measure of the total area for both components. This relative number for each component was taken as a measure for the relative amount of action potentials contributing to the component.

For automatic peak fitting, mathematical techniques were used to determine the relative contribution of the area under both components. Using the multi-peak fitting algorithm in Igor (http://www.wavemetrics.com) the peaks were fitted automatically. The results were confirmed with the multi-peak fitting algorithm of Origin (http://www.originlab.com).

For each bimodal activity pattern, area approximation was performed by fitting two or more Gaussian functions to the smoothed signal. Usually, these

Gaussian functions are added to a baseline. In figure 4.3 B for example, the two Gaussian functions which describe the smoothed signal must be added to a baseline. In figure 4.3 B, the baseline is set at a constant level $f(x) = 135$. If no baseline function was used in the fitting procedure, the fitting algorithm often added an extra Gaussian function which served as a baseline. Three types of baseline functions were used. The first baseline function was a constant level ($f(x) = a$), the second a linear function ($f(x) = a + bx$) and the third baseline function was a cubic function ($f(x) = a + bx + cx^2 + dx^3$). No quadratic function was used because the results were very similar to either the linear or the cubic function. In addition to fitting the complete curve, we also fitted a part of the smoothed signal that only contained both components. The resulting Gaussian functions that best described the two peaks of the components were selected, using the lowest chi-square test statistic and the lowest Akaike Information Criterion (AIC) value. The area for the selected peaks was subsequently determined and then regarded relative to the total area for both components. These relative values were taken as an indication for the relative number of action potentials contributing to each component.

The Gaussian function describing the component peaks was characterized as follows

$$y = \frac{A}{w}\sqrt{(\pi/2)}e^{-2(\frac{x-x_c}{w})^2}, \qquad (1)$$

where A represents the area under one Gaussian, w characterizes the width of the Gaussian function, and x_c represents the time of the peak of the Gaussian function.

4.2.5 Simulation studies

Simulations were done in the Matlab programming environment (Matlab, 2007) using the model that was described in chapter 3, section 3.2. Two components were simulated at the average ZT times of the unshifted and shifted component (ZT 9 and ZT 13, ZT before the shift). The multiunit activity pattern was derived from the activity patterns of the two components. Each component was composed as an ensemble of neurons, by distributing a number of single unit activity patterns according to the

following Gaussian distribution $e^{-(x-\mu)^2/2\sigma^2}$. The single unit pattern was obtained by taking the average electrical activity of recorded single unit patterns, as described in (VanderLeest et al., 2007;Rohling et al., 2006a). The number of neurons and the width of the distribution could be adjusted for each component separately. Sigma (σ) of a distribution is a measure for the width of a Gaussian distribution, a high sigma reflecting a broad distribution and a small sigma indicating a narrow distribution.

4.3 Results

Albus et al. (2005) witnessed two components in the multiunit activity pattern after a 6 h delay of the light-dark cycle. One component was situated in the ventrolateral region of the SCN, while the other resided in the dorsomedial region. The two components could be identified by two separate peaks of electrical activity in multiunit recordings. On day 1 after the delay, the two peaks were already clearly distinguishable. Additional electrophysiological experiments have been carried out to obtain a sufficient amount of data for the quantitative analysis of the observed bimodal pattern.

The experiments for day one after the delay used in Albus et al. (2005) were pooled with the new experiments. From all experiments, 13 showed two components in the recording. Looking at these examples there was a clear tendency that the peak of the shifted component was more narrow than the peak of the unshifted component (figure 4.1). First, we confirmed the difference in the shift of the two components, as found in Albus et al. (2005) (figure 4.2 B). Then, the width of the peaks at the level of the trough between both peaks was measured (figure 4.2 A). The width of the shifted component was significantly narrower than the width of the unshifted component ($p < 0.001$; figure 4.2 C), and this was also true when the relative widths were compared ($p < 0.001$).

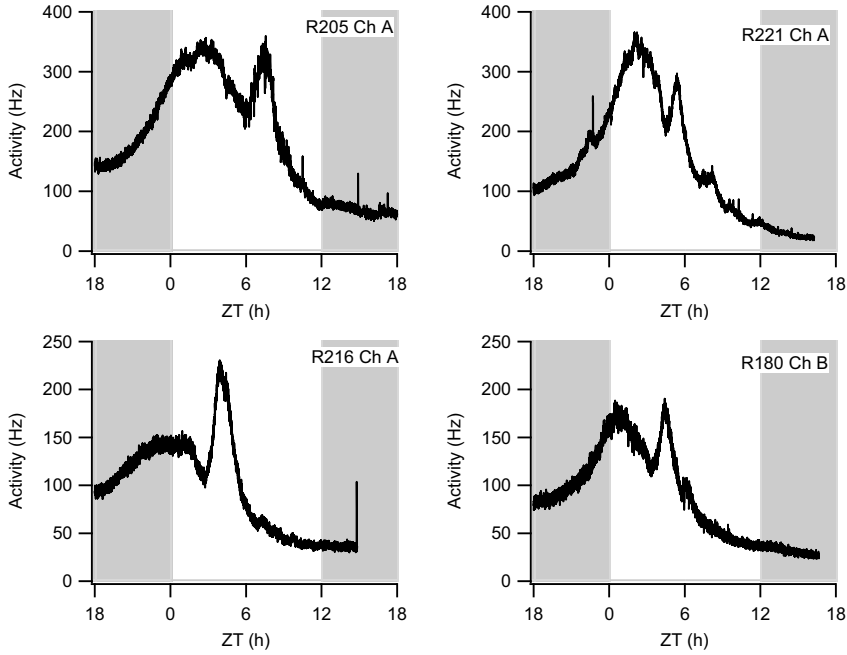

Figure 4.1 Four examples of recordings showing two components. Multiunit electrical activity recordings clearly showing two peaks in electrical activity. The shifted light-dark schedule is depicted with gray indicating the night. The left peak in each recording is unshifted component, while the right peak is the shifted component.

Next, we manually fitted the smoothed patterns to determine the area under the curves for both components and calculated the relative contribution of each (figure 4.3 A). The results were a rough estimate of the area for each curve and showed that the area of the unshifted component was about 70% and the area of the shifted component about 30% (figure 4.3 C).

In the manual fits, the shape of the curve was not considered, which puts a bias on the smaller shifted component. To avoid this bias, we fitted two or more Gaussian functions to the smoothed pattern using the automatic fitting procedures. The best fit was used and the Gaussian curves for both components were analyzed (figure 4.3 B). The areas for both components were again determined relative to each other. The first component was almost 80%, while the area of the second component was 20% (figure 4.3 D).

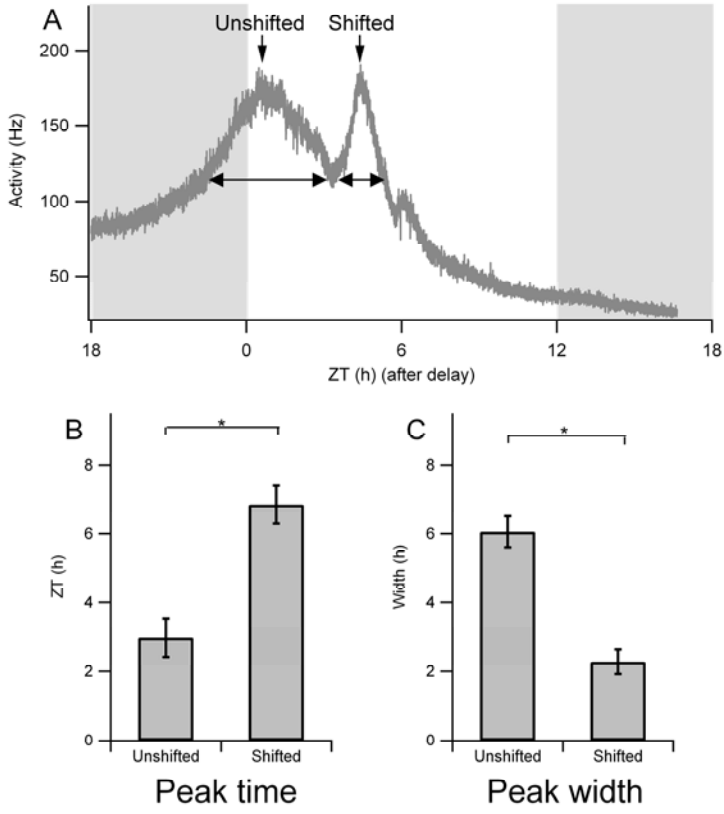

Figure 4.2 Width and time of peak for both components. (A) Raw multiunit activity recording following a shift of the light-dark cycle. After smoothing of the data, the trough between both components was determined as well as the peak times. Subsequently, the width of the unshifted and the shifted component was determined by drawing a horizontal line from the trough to the opposing slope of the component's peak. (B) The peak time for the shifted component occurred at ZT 3.0 ± 2.0 h, while the unshifted component peaked at ZT 6.8 ± 2.0 h. The ZT refers to the shifted Zeitgeber time. The difference in peak times was statiscally significant ($p < 0.01$). (C) The width of the peak of the unshifted component was 6.1 ± 1.6 h, while the shifted component had a peak width of 2.3 ± 1.3 h. This was also significantly different ($p < 0.01$).

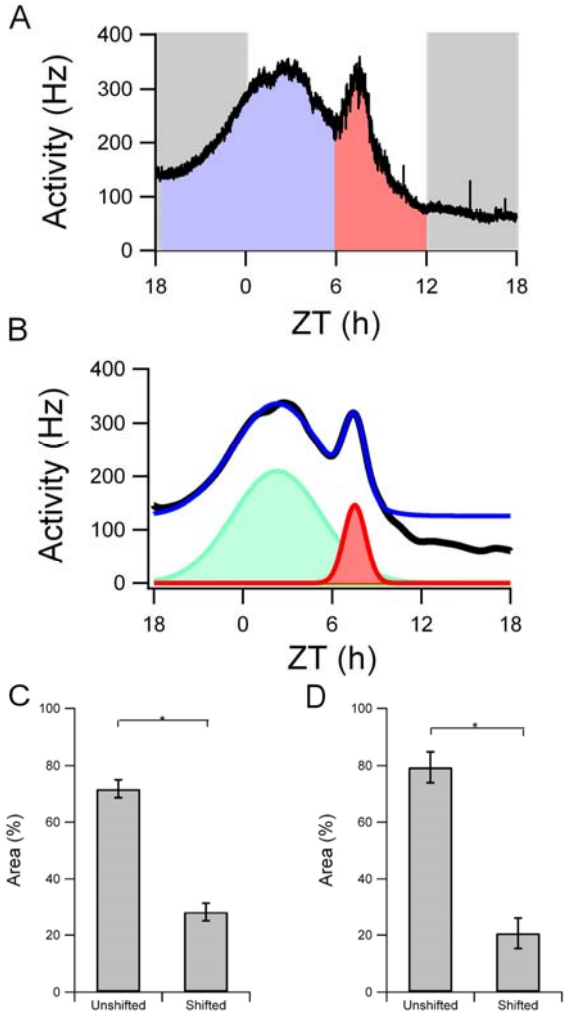

Figure 4.3 Relative number of action potentials contributing to each component. The area under the curve for each component was taken as an indication for the amount of action potentials contributing to each component. (A) The total area under each of the components was used to determine the relative number of action potentials contributing to each component. (B) Mathematically fitting Gaussian functions to the smoothed multiunit activity pattern also gave an indication of the area under each component peak. (C) The area under the unshifted component as determined in (A) was about 70% of the total area, while the area under the shifted component was 30%. (D) For mathematical fitting, about 80% of the relative area under both components was covered by the unshifted component and 20% was covered by the shifted component.

Finally, we used a subpopulation analysis to determine the number of subpopulations in the unshifted and shifted component. Subpopulation analysis shows the time of the peak of subpopulations in the recording. The peak times of these subpopulations were determined relative to the time of the trough between both components. The subpopulation analysis shows that more subpopulations were present before the trough than after the trough (figure 4.4). Before the trough, a total number of 37 subpopulations were observed and after the trough 12 subpopulations were observed. The distribution of the subpopulations found before the trough is significantly broader than after the trough ($p < 0.05$).

From these results it seems that only a relatively small group of neurons shifts immediately after a 6-hour phase delay. The group of shifted neurons also appears to have a narrower phase distribution as compared to the unshifted group. To obtain more insight in the mechanism that can explain this phenomenon, simulations were performed.

In the simulations, the multiunit pattern shows a bimodal pattern if the width of the shifted component was considerably smaller than the width of the unshifted component (or vice versa). Also, in the case of the two components that are separated only by 4 hours, the number of neurons contributing to the shifted components had to be less than the number contributing to the unshifted component (or vice versa). When these prerequisites were met, a bimodal multiunit activity pattern was obtained (figure 4.5 A and B). When the distribution of the shifted component is narrowed, the number of neurons contributing to the shifted component can be varied slightly, although they should not be more than 30% of the total amount of neurons. This small variability in the amount of neurons in the shifted component produces different shapes of bimodal peaks (figure 4.5 C and D), that can also be found in the experimental data (figure 4.1). If the number of neurons contributing to the shifted component is about 20% of the total amount of neurons a bimodal shape in the multiunit activity pattern is found where the height of the peak of the shifted component is similar to that of the unshifted component (figure 4.5 D). However, if the percentage is higher, the height of the shifted peak immediately increases substantially as opposed to the unshifted one (figure 4.5 C).

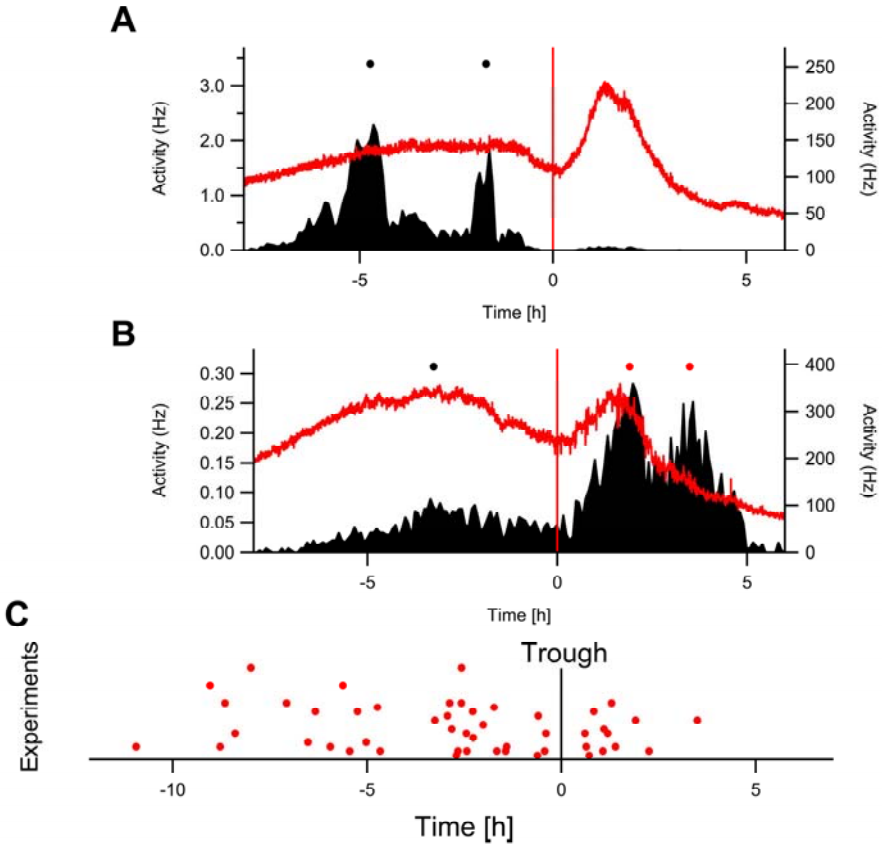

Figure 4.4 Subpopulation analysis of the shifted electrical activity profile. (A and B) The multiunit activity pattern (right axis) and subpopulations (left axis) for the same recording. The peak times of the subpopulations were determined by smoothing the electrical activity pattern. The dots denote the times of the peaks of the subpopulations. The subpopulation analysis was performed for all bimodal recordings and for all experiments the peak times were aligned to the trough (C). The number of subpopulations found in the unshifted component was higher than that in the shifted component (80 % versus 20 % respectively). Furthermore, the subpopulations of the unshifted component show a much broader distribution than the subpopulations of the shifted component.

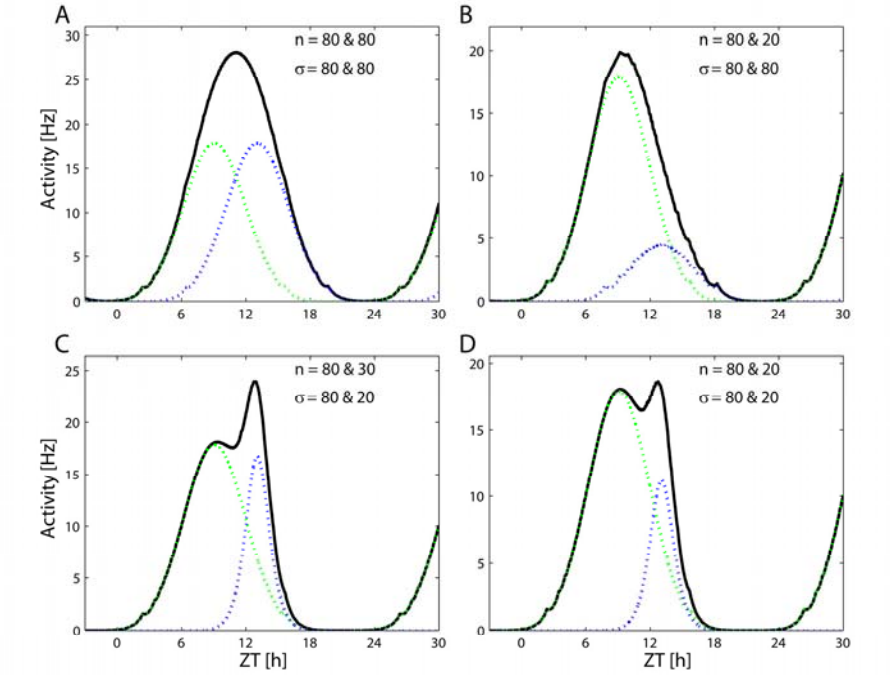

Figure 4.5 Simulations of electrical activity patterns with two components. Each graph shows the resulting multiunit pattern of two components that are placed at ZT 9 and ZT 13. Each component contains a number of neurons and these neurons are distributed according to a Gaussian distribution that has a certain width (indicated by σ: a lower value leads to a narrow distribution). (A) Both populations have an equal number of neurons and the same distribution. This leads to a single peak in the multiunit activity pattern. (B) The number of neurons in the second component is decreased, still resulting in a unimodal multiunit pattern. (C and D) The distribution of the shifted component is narrower. This leads to a bimodal multiunit pattern. If the number of neurons in the unshifted component is 80% and in the shifted component 20%, the obtained multiunit activity pattern resembles recorded bimodal multiunit activity patterns. (C). If the number of neurons is increased only by a small amount, we see that the second peak rapidly becomes higher (D). We have also seen this in one of the recordings (figure 4.1 C).

While we can not be certain of other mechanisms that might be involved in the shift of the light-dark cycle for different parts of the SCN, we have shown that the unshifted component is broader than the shifted component. The unshifted component also contributes more to the total activity of the multiunit pattern than the shifted component, and the number of subpopulations is higher in the unshifted component. The subpopulations in the shifted component are more clustered in phase.

4.4 Discussion

New experiments were performed to explore the mechanisms involved in the dissociation of neuronal subpopulations in the SCN after a phase delay of 6 hours. At day one after the shift, two components could be identified in the electrical activity pattern. First, we analyzed these bimodal patterns by measuring the width of both components and observed that the width of the unshifted component was substantially broader than the width of the shifted component. The width of the unshifted component was almost three times as broad as the width of the shifted component.

Then, we calculated the relative contributions of each component to the ensemble pattern by the use of curve fitting methods and a subpopulation analysis. We found that only a small percentage (20-30 %) of the total number of action potentials shifted immediately after the delay of 6 hours, while the larger part of the action potentials contributed to the unshifted component. The data suggest that only a small number of the total population of neurons shifted immediately following the delay.

Using simulations, we investigated how the activity patterns for two subpopulations can lead to bimodal ensemble patterns. In simulation studies, discussed in chapter 3 (sections 3.3.3 and 3.4.3), it was found that the width of the distributions for each component had to be narrow and the components had to be sufficiently separated in time to render a bimodal pattern. In the present study, our simulations show that also the relative number of neurons is of importance. Our simulations show that bimodal patterns in multiunit activity only arise when two conditions are met. First, the width of the distribution of the shifted component is maximally 25 % of the distribution width of the unshifted component. Second, the number of neurons contributing to the shifted component is maximally 25 % of the amount contributing to the unshifted component. If these conditions are not met, the multiunit activity pattern shows only one peak.

Some of our recordings showed one peak in electrical activity. This does not necessarily reflect a unimodal distribution of the contributing neurons. As shown in figures 4.5 A and B, bimodal distributions can result in unimodal multiunit activity patterns. For the unimodal recordings, the distribution of the shifted component may have been broad or the

components were not separated enough in time (see chapter 3, sections 3.3.3 and 3.4.3). Either case results in a unimodal multiunit activity pattern.

In a previous paper, Albus et al (2005) found that the two concurrent peaks in the in vitro electrical activity measurements could be located in the ventral and dorsal SCN. The ventral SCN is shifted immediately to the new phase, while in the dorsal SCN the shift is completed only after 6 days. We expect that the small group of rapidly shifting neurons is located in the ventral SCN.

In the current study we restricted ourselves to phase delays. Phase advances of the circadian system are known to be more complex, and require more time, than phase delays. In vitro electrical activity measurements in the rat SCN, following 6 hour phase advances showed an immediate shift of about 3 hours, but after 6 days the phase was at the old regime again (no phase shift persisted: Vansteensel et al., 2003). In vivo electrical activity showed no phase shift after a phase advance, indicating that perhaps the dorsal SCN does not shift and keeps the ventral SCN from shifting too (Vansteensel et al., 2003). When dorsal and ventral SCN in vitro after an advance where measured, there was indeed a difference in the phase shift: the ventral SCN shifted more quickly than the dorsal (Albus et al., 2005). This indicates that also for advances the dorsal and ventral region of the SCN shift at a different pace, causing dissociation within the SCN.

In molecular studies, different clock genes have been assessed following a phase delay or advance of the light-dark cycle. The expression of Per1 showed a rapid phase shift immediately after a delay or an advance (Reddy et al., 2002;Nagano et al., 2003;Yamazaki et al., 2000;Vansteensel et al., 2003). However, in different regions of the SCN, the response was different. In the ventral part of the SCN the shifts were immediate, while in the dorsal part the shift took longer (Nagano et al., 2003). Even within the ventral and dorsal regions, differences in phase shifting capacity of Per1 were found, where lateral cells shifted more rapidly than medial cells (Nakamura et al., 2005). Furthermore, an advance was more difficult than a delay (Nagano et al., 2003;Nakamura et al., 2005). Per2 expression showed the same characteristics as Per1 (Reddy et al., 2002;Nagano et al., 2003). This

indicates that also in gene expression a dissociation exists between the ventral and the dorsal SCN.

Apart from regional differences there are differences in the adaptation rate of certain clock genes. During phase delays, the Cry1 gene expression was synchronized to the expression of Per1 and Per2 (Reddy et al., 2002). Following phase advances the Cry1 gene expression rhythm became out of phase with the expression of Per1 and Per2 genes (Reddy et al., 2002). CRY1 protein levels followed the Cry1 gene expression profiles for phase delays (Nagano et al., 2003). This might indicate a special role for Cry1 in the phase resetting properties of the SCN, which differs between delays and advances.

In conclusion, we propose that phase shifts are brought about by an initial rapid shift of a relatively small subpopulation of neurons within the SCN. This group resides most probably in the ventral part of the SCN. Coupling between the shifted and the unshifted population of SCN neurons is asymmetrical, as the shifted neurons exert a strong phase shifting effect on the unshifted neurons. This causes a complete shift of the SCN which is realized after several cycles.